SCIENCE CHINA
Chemistry

•ARTICLES•

December 2021 Vol.64 No.12: 2154–2160
https://doi.org/10.1007/s11426-021-1082-7

Molecular rotors as a class of generally highly active ion transporters

Jie Shen[1], Joan Jia Ying Han[2], Ruijuan Ye[1] & Huaqiang Zeng[1*]

[1]*Frontier Research Center for Multidisciplinary Sciences, School of Chemistry and Chemical Engineering, Northwestern Polytechnical University, Xi'an 710072, China;*
[2]*Temasek Polytechnic, 21 Tampines Avenue 1, Singapore 529757, Singapore*

Received May 5, 2021; accepted August 3, 2021; published online October 27, 2021

We describe here a class of unconventional ion transporters, molecular rotors that transport ions through a rotating function rather than *via* traditional carrier or channel mechanisms. Mimicking macroscopic rotors, these molecular rotors consist of three modularly tunable components, *i.e.*, a membrane-anchoring stator, a crown ether-containing rotator for ion binding and transport, and a triple bond-based axle that allows the rotator to freely rotate around the stator in the lipid membrane. Lipid bilayer experiments reveal the generally high ability of all molecular rotors in promoting the highly efficient transmembrane K^+ flux (EC_{50} values = 0.49–1.37 mol% relative to lipid). While molecular rotors differing only in the ion-binding unit exhibit similar ion transport activities, those differing in the rotator's length display activity differences by up to 174%.

supramolecular chemistry, molecular machines, artificial membrane transporters, molecular rotors, K^+ transporters

Citation: Shen J, Han JJY, Ye R, Zeng H. Molecular rotors as a class of generally highly active ion transporters. *Sci China Chem*, 2021, 64: 2154–2160, https://doi.org/10.1007/s11426-021-1082-7

1 Introduction

In nature, biological molecular machines widely known to science include myosin that contracts and relaxes muscle [1], kinesin that moves cellular cargo around the cell [2] and helicase that unwinds double-stranded DNA [3]. Fascinated but challenged by the sheer complexity of these naturally occurring molecular machines, chemists have been taking a minimalist approach in creating diverse types of nanometer-sized artificial molecular machines (AMMs) over the past decades [4–6], and promising many possible applications in developing the next-generation nanoscale electronics. These AMMs are structurally much simpler but come with the built-in ability to perform macroscopic mechanical movements as seen in molecular shuttle [4], switch [5], muscle [6,7], rotor/motor [5], propeller [8], pump [9], walker [10], mover [11], nanocar [12], synthesizer [13], balance [14], *etc*. Although artificial molecular rotors/motors have received intensive attention among the scientific community, their possible role as membrane transporters has yet not been investigated.

On the other hand, it has been recently demonstrated that AMM-inspired ion transporters, such as molecular shuttle [15], molecular swing [16], molecular ion fisher [17], molecular tetrahedron [18] and molecular ball [19] can be employed to mediate efficient ion transport across the membrane *via* shuttling, swing, ion-fishing or swing/relay actions. These unconventional ion transport mechanisms differ drastically from traditional carrier [20–23] or channel [24–48] mechanisms for transmembrane ion transport. Adding into a growing list of AMM-inspired unconventional ion transporters and mechanisms, in this article, we show that appropriately designed molecular rotors (MRs) could also function well in a lipid bilayer membrane.

*Corresponding author (email: hqzeng@nepu.edu.cn)

2 Experimental

2.1 General remarks

All the reagents were obtained from commercial suppliers and used as received unless otherwise noted. Aqueous solutions were prepared from MilliQ water. The organic solutions from all liquid extractions were dried over anhydrous Na_2SO_4 for a minimum of 15 min before filtration. Chemical yield refers to pure isolated substances. ^1H and ^{13}C NMR spectra were recorded on a Bruker ACF400 spectrometer (Germany). ^{13}C spectra are proton-decoupled and recorded on Bruker ACF400 (400 MHz). Mass spectra were acquired with Thermo Scientific Exactive LC-MS (USA).

2.2 Synthesis and characterization

Molecular rotors were synthesized *via* the synthetic route outlined in the Supporting Information online. All the intermediates and final products were fully characterized with ^1H NMR, ^{13}C NMR and MS.

2.3 Ion transport study using the HPTS assay and EC_{50} measurements using the Hill analysis

Egg yolk L-α-phosphatidylcholine (EYPC, 0.6 mL, 25 mg/mL in $CHCl_3$, Avanti Polar Lipids, USA) was added into a round-bottom flask. The solvent was removed under reduced pressure at 30 °C. After being dried overnight under high vacuum, the film was hydrated with 4-(2-hydroxyethyl)-1-piperazine-ethane sulfonic acid (HEPES) buffer solution (3 mL, 10 mM HEPES, 100 mM NaCl, pH 7.0) containing a pH-sensitive dye 8-hydrox-ypyrene-1,3,6-trisulfonic acid (HPTS, 1 mM) in thermostatic shaker-incubator at 25 °C for 2 h to give a milky suspension. The mixture was then subjected to 10 freeze-thaw cycles: freezing in liquid N_2 for 1 min and heating with the 37 °C water bath for 2 min. The vesicle suspension was extruded through polycarbonate membrane (0.1 μm) to produce a homogeneous suspension of large unilamellar vesicles (LUVs) of about 120 nm in diameter with HPTS encapsulated inside. The suspension of LUVs was dialyzed for 16 h with gentle stirring (300 r/min, 4 °C) using membrane tube (MWCO = 10,000) against the same HEPES buffer solution (300 mL, without HPTS) for 8 times to remove the unencapsulated HPTS, yielding LUVs with lipids at a concentration of 6.5 mM.

The HPTS-containing LUV suspension (30 μL, 6.5 mM in 10 mM HEPES buffer containing 100 mM NaCl at pH 7.0) was added to a HEPES buffer solution (1.90 mL, 10 mM HEPES, 100 mM MCl at pH 8.0, where $M^+ = Li^+$, Na^+, K^+, Rb^+, and Cs^+) to create a pH gradient for ion transport study. A solution of channel molecules in dimethyl sulfoxide (DMSO) was then injected into the suspension under gentle stirring. Upon the addition of channels, the emission of HPTS was immediately monitored at 510 nm with excitations at both 460 and 403 nm recorded simultaneously for 300 s using fluorescence spectrophotometer after an aqueous solution of Triton X-100 was added to achieve the maximum change in dye fluorescence emission. The final transport trace was obtained after subtracting background intensity at $t = 0$, as a ratiometric value of I_{460}/I_{403} and normalized based on the ratiometric value of I_{460}/I_{403} after addition of triton. The fractional change R_{M^+} was calculated for each curve using the normalized value of I_{460}/I_{403} at 300 s before the addition of triton, taking triton with the ratiometric value of I_{460}/I_{403} at $t = 0$ s as 0% and that of I_{460}/I_{403} at $t = 300$ s (obtained after addition of triton) as 100%. Fitting the fractional transmembrane activity R_{M^+} *vs*. channel concentration using the Hill equation: $Y=1/(1+(EC_{50}/[C])^n)$ gave the Hill coefficient n and EC_{50} values.

2.4 Chloride transport using the SPQ assay

Egg yolk L-α-phosphatidylcholine (EYPC, 0.6 mL, 25 mg/mL in $CHCl_3$, Avanti Polar Lipids, USA) was added into a round-bottom flask. The solvent was removed under reduced pressure at room temperature. After being dried overnight under high vacuum at room temperature, the film was hydrated with $NaNO_3$ solution (3 mL, 200 mM) containing a Cl-sensitive dye 6-methoxy-*N*-(3-sulfopropyl)quinolinium (SPQ, 0.5 mM) in thermostatic shaker-incubator at 25 °C for 2 h to give a milky suspension. The mixture was then subjected to 10 freeze-thaw cycles: freezing in liquid N_2 for 30 s and heating at 37 °C for 2 min. The vesicle suspension was extruded through polycarbonate membrane (0.1 μm) to produce a homogeneous suspension of large unilamellar vesicles (LUVs) of about 120 nm in diameter with SPQ encapsulated inside. The suspension of LUVs was dialyzed for 16 h with gentle stirring (300 r/min, 4 °C) using membrane tube (MWCO =10,000) against the same $NaNO_3$ buffer solution (200 mM, without SPQ) for 8 times to remove the unencapsulated SPQ, yielding LUVs with lipids at a concentration of 6.5 mM.

The SPQ-containing LUV suspension (30 μL, 6.5 mM in 200 mM $NaNO_3$) was added to a NaCl solution (1.90 mL, 200 mM) to create an extravesicular chloride gradient. A solution of our sample in DMSO at different concentrations was then injected into the suspension under gentle stirring. Upon the addition of channels, the emission of SPQ was immediately monitored at 430 nm with excitations at 360 nm for 300 s using fluorescence spectrophotometer after an aqueous solution of Triton X-100 (20 μL, 20% *v*/*v*) was added to completely destruct the chloride gradient. The final transport trace was obtained by normalizing the fluorescence intensity using the Eq. (1):

$$I_f = [(I_t - I_1)/(I_0 - I_1)] \quad (1)$$

where I_f: fractional emission intensity, I_t: fluorescence intensity at time t, I_1: fluorescence intensity after addition of Triton X-100, and I_0: initial fluorescence intensity.

2.5 Membrane leaking and pore size determination using CF dye

Egg yolk L-α-phosphatidylcholine (EYPC, 0.6 mL, 25 mg/mL in $CHCl_3$, Avanti Polar Lipids, USA) was added into a round-bottom flask. The solvent was removed under reduced pressure at 30 °C. After being dried overnight under high vacuum at room temperature, the film was hydrated with HEPES buffer solution (1 mL, 10 mM HEPES, 100 mM NaCl, pH 7.5) containing a 5(6)-fluorescein (CF, 50 mM) in thermostatic shaker-incubator at 25 °C for 2 h to give a milky suspension. The mixture was then subjected to 10 freeze-thaw cycles: freezing in liquid N_2 for 1 min and heating at 37 °C in the water bath for 2 min. The vesicle suspension was extruded through polycarbonate membrane (0.1 μm) to produce a homogeneous suspension of LUVs of about 120 nm in diameter with CF encapsulated inside. The suspension of LUVs was dialyzed for 16 h with gentle stirring (300 r/min, 4 °C) using membrane tube (MWCO=10,000) against the same buffer solution (HEPES buffer with 100 mM NaCl, pH 7.5) for 8 times to remove the unencapsulated CF dye, yielding LUVs with lipids at a concentration of 6.5 mM.

The CF-containing LUV suspension 30 μL, 6.5 mM in 10 mM HEPES buffer containing 100 mM NaCl at pH 7.5) was added to a HEPES buffer solution (1.90 mL, 10 mM HEPES, 100 mM NaCl at pH 7.5) to create a concentration gradient for CF dye transport study. A solution of our samples or natural pore-forming peptide Melittin in DMSO at different concentrations was then injected into the suspension under gentle stirring. Upon the addition of channel molecules, the emission of CF was immediately monitored at 517 nm with excitations at 492 nm for 300 s using fluorescence spectrophotometer after an aqueous solution of Triton X-100 (20 μL, 20% *v*/*v*) was added to completely destruct the chloride gradient. The final transport trace was obtained by normalizing the fluorescence intensity using Eq. (1).

3 Results and discussion

3.1 Molecular design of molecular rotors

A molecular rotor comprises two parts—a membrane-spanning stator and a rotator, both of which are rotatable relative to each other *via* a connecting axle. In our modular molecular design as illustrated in Figure 1, a bis-cholesterol segment of 40 Å in length, containing two hydroxyl-rich cholesterol groups covalently linked through a rigid symmetric isophthalohydrazide linker, was used as the stator whose membrane-spanning ability has been verified previously [16]. This helps to orient the rotator, which contains a flexible linear alkyl linker of 3 to 6 carbon atoms and a crown ether unit for ion binding and transport, in parallel with the membrane axis and the hydrophobic membrane tails to perform their intended functions. Moreover, since this cholesterol-containing stator will associate with the hydrophobic lipid tails more tightly than the crown ether-containing rotator, rotation involving the rotator around the stator should be more frequent and more likely than the other way around. To attain good ion transport activities in the lipid membrane, internal rotation around the axle is expected to be as frictionless as possible so that **MR**s can reorient easily at room temperature. In this regard, an axle made of an almost freely rotatable triple bond, which has a low rotational energy barrier of 0.4−1.1 kcal/mol [49], appears to be an ideal choice.

Using this modularly tunable structural scheme, we designed and prepared one series of 15-crown-5 unit-containing **MR5**s and another series of 18-crown-6 unit-containing **MR6**s. To probe the length effect of the rotator, each series consists of four **MR**s, having a flexible linker of 3 to 6 carbon atoms (*e.g.*, **C3** to **C6**) and a tunable rotator length of 12–16 Å. For comparison purpose, control compounds **Cr1** and **Cr2** (Figure 1), made of a single stator or rotator component, were also prepared.

3.2 High transport activity with good K^+/Na^+ selectivity

It is well known that the energetic penalty for cations reaches the highest when they are in the membrane's center. Thus, it remains curious to us whether these **MR**s will be able to compensate for this energy penalty and move the ion from one side of the membrane to the other side along the ionic concentration gradient. The hypothetic **MR**-mediated ion transport was examined using a well-established pH-sensitive HPTS assay, with the extravesicular region containing 100 mM MCl (M = Li, Na, K, Rb and Cs, Figure 2a). In the particular case of potassium transport (Figure 2b), we found that **MR5-C5** and **MR6-C5** display the highest transport activities, exhibiting respective R_{K^+} (fractional ion transport activity) values of 99% and 93% at 1 μM which correspond to a molecular rotor:lipid molar ratio of 1 mol%. The fact that, at the same concentration, the R_{K^+} values for control compounds **Cr1** and **Cr2** are less than 4% after subtracting the background signal (Figure 2b) points to the critical role synergistically played by both stator and rotator, allowing the rotator to rotate around the axle and stator to achieve highly efficient transport of potassium; in the absence of either component, however, either stator (**Cr1**) or the rotator (**Cr2**) alone can only act as the extremely weak ion transporters almost incapable of moving potassium ions

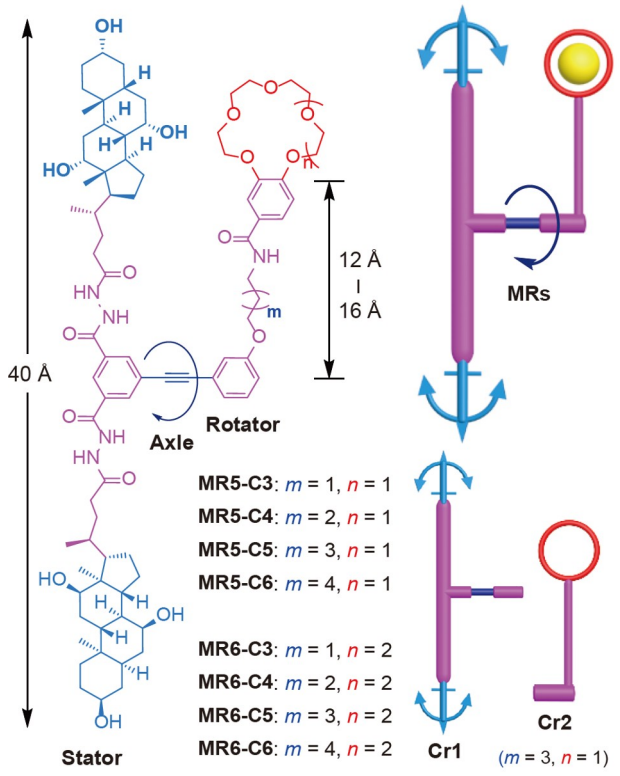

Figure 1 Molecular design of molecular rotors **MR5**s and **MR6**s, made up of a cholesterol-containing stator, a crown ether-containing rotator and an axle derived from an almost freely rotatable triple bond (color online).

across the membrane.

Recently, we found that the membrane dialysis method to remove the unencapsulated HPTS dye consistently produces tight LUVs with low background signals (*e.g.*, 3.2% for K^+, 4.0% for Na^+ and < 8% for Li^+, Rb^+ and Cs^+) [17,35]. Employing these low background LUVs, we performed the Hill analyses and determined the EC_{50} values for Na^+ and K^+ ions for all **MR**s (Table 1 and Figures S1–S8, Supporting Information online). Based on these EC_{50} values, (1) all **MRs** are highly active in transporting both Na^+ and K^+ ion, with EC_{50} values of ≤ 2.29 μM (2.29 mol% relative to lipid), (2) all **MR**s are weakly or moderately K^+-selective, with K^+/Na^+ selectivity values of 1.2–3.7, (3) the best Na^+ and K^+ transporters are **MR6-C3** and **MR5-C5**, respectively, and (4) coincidentally, the best K^+ transporter **MR5-C5** happens to be the most selective among the eight **MR**s.

Previously, we demonstrated that the ratio of fractional ion transport activities R_{M^+} (*e.g.*, R_{K^+}/R_{Na^+}) could serve as a reliable index for evaluating ion transport selectivity [17,35], a method that not only complements but also might be more accurate in many cases than the use of EC_{50} values. Its high reliability was further verified very recently by Li *et al.* [43]. Accordingly, by varying the extravesicular salts MCl (M = Li, Na, K and Rb, Figure 2a), we have measured all R_{M^+} values for all eight **MR**s (Figures 2c and S9, S10). These R_{M^+} values clearly show that all **MR**s transport K^+ ions faster than any of the other four cations. Particularly, the ratios of R_{K^+}/R_{Na^+} are highly consistent with the ratios of EC_{50} values (Table 1). From this finding, we can conclude that the ratio **R** (*e.g.*, R_{K^+}/R_{Na^+}) is a more preferred method for selectivity assessment than EC_{50} values due to its simplicity and broader applicability to the cases where ion transporters are not very active or have relatively poor solubility and thus EC_{50} values cannot provide a reliable assessment [17,35]. It would be worth emphasizing that all R_{M^+} (R_{K^+}, R_{Na^+}, *etc.*) values should be determined not only at the same concentration but also at the concentration where the transporter elicits a fractional transport activity of close to 100% over a duration of 300 s for the most active ion (*e.g.*, potassium ion in our case, Figures 2c and S9, S10), in order to obtain reliable R_{M^+} and ratio **R** values for an accurate assessment of ion transport selectivity.

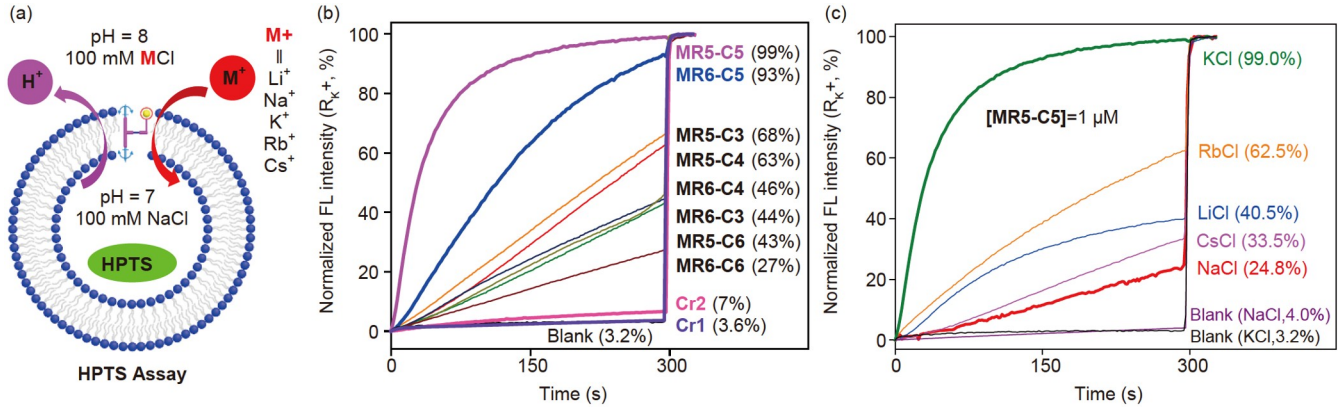

Figure 2 (a) Schematic illustration of the pH-sensitive HPTS assay, with extravesicular salt MCl variable, for comparing ion transport activities of **MR**s. (b) Fractional potassium transport activities, which were determined over 5 min at 1 μM, with the extravesicular region containing 100 mM KCl. $R_{K^+}=(I_{K^+}-I_0)/(I_{triton}-I_0)$ wherein I_{K^+} and I_0 (background intensity) are the ratiometric values of I_{460}/I_{403} at t = 300 s before addition of triton and I_{triton} is the ratiometric value of I_{460}/I_{403} at t = 300 s right after addition of triton. (c) Fractional ion transport activities, which were determined over 5 min at 1 μM of **MR5-C5**, with the extravesicular region containing 100 mM MCl (M = Li, Na, K, Rb and Cs). $R_{M^+}=(I_{M^+}-I_0)/(I_{triton}-I_0)$. [Total lipid] = 100 μM (color online).

Table 1 Determined values for EC_{50} (μM), $EC_{50}(Na^+)/EC_{50}(K^+)$ and R_{K^+}/R_{Na^+}

	MR5-C3	MR5-C4	MR5-C5	MR5-C6	MR6-C3	MR6-C4	MR6-C5	MR6-C6
$EC_{50}(Na^+)$[a)]	1.38 ± 0.03	1.62 ± 0.12	1.81 ± 0.12	2.29 ± 0.08	1.22 ± 0.03	1.51 ± 0.06	1.67 ± 0.11	2.77 ± 0.20
$EC_{50}(K^+)$[a)]	0.76 ± 0.03	0.81 ± 0.03	0.49 ± 0.03	1.13 ± 0.04	1.03 ± 0.04	1.00 ± 0.04	0.50 ± 0.04	1.37 ± 0.05
$EC_{50}(Na^+)/EC_{50}(K^+)$	1.8	2.0	3.7	2.0	1.2	1.5	3.3	2.0
R_{K^+}/R_{Na^+} [b)]	1.8	2.1	4.0	1.8	1.1	1.4	3.2	2.3

a) [Total lipid] = 100 μM. b) See Figures 2c and S9, S10 for more detail.

3.3 Transport mechanism study

Having identified **MR5-C5** as the most active (EC_{50} = 0.49 μM = 0.49 mol% relative to lipid, Table 1) and selective (K^+/Na^+ = 4.0, Table 1) potassium transporter, we applied it to elucidate the possible transport species (M^+ or X^-) and mechanism (M^+/H^+ antiport, X^-/OH^- antiport, M^+/OH^- symport, or X^-/H^+ symport).

We first used the chloride-sensitive SPQ assay to examine which ionic species (X^- or M^+) is involved in the **MR**-mediated ion transport process. SPQ is a dye whose fluorescence decreases with increasing Cl^- concentrations, and continuous influx of Cl^- anions therefore will result in continuous decreases in fluorescence intensity of SPQ. Using this assay, while the anion channel **L8** previously developed by us [37] effects an overall reduction of fluorescence intensity by 67% over 300 s at 1 μM, **MR5-C5** (Figure 3a) and the other seven **MR**s (Figure S11) cause no significant fluorescence quenching at the same concentration. These comparable data undoubtedly establish M^+, rather than X^-, as the transport species (Figure 3a).

Next, we used **FCCP** (a known proton carrier) to compare the transmembrane transport rates between M^+ and H^+ (Figure 3b). If **MR**-promoted transport of M^+ (*e.g.*, K^+) is faster than that of H^+ or OH^-, the addition of **FCCP** will speed up proton efflux in order to maintain the charge neutrality of the system, subsequently leading to enhanced fluorescence of the HPTS dye. Indeed, we observed a net increase of 46% in fluorescence intensity in the absence (34%) and presence (80%) of **FCCP** for the same **MR5-C5**-mediated potassium transport process over the same duration of 300 s. Given that fluorescence intensity for **FCCP** alone (4.1%) differs marginally from the background signal (3.2%), an increase of 46% confirms transport of either H^+ or OH^- to be the rate-limiting step. We can draw the same conclusion for the remaining seven **MR**s (Figures S12, S13).

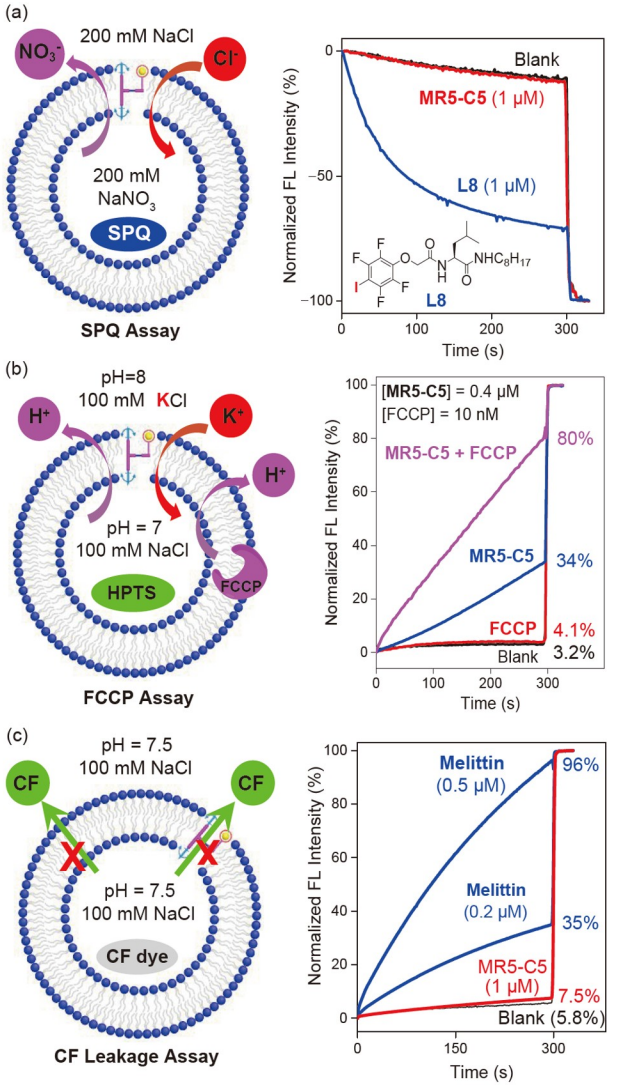

Figure 3 (a) Chloride-sensitive SPQ assay, confirming that **MR5-C5** does not transport anions; **L8** is an anion channel [37]. (b) FCCP-based HPTS assay, employing proton carrier FCCP to establish transmembrane transport of either proton or hydroxide ions as the rate-limiting step. (c) CF-leakage assay, suggesting membrane integrity in the presence of **MR5-C5** (color online).

3.4 Membrane integrity in the presence of MRs

We used the carboxyfluorescein (CF)-leakage assay (λ_{ex} = 492 nm, λ_{em} = 517 nm, Figure 3c) to check the membrane integrity in the presence of these molecular rotors. Having the smallest dimension of 0.9 nm (Figure S14), fluorescent CF dye exists mostly as a non-fluorescent dimer at high concentrations (*e.g.*, 50 mM as used in our CF assay). Thus, any membrane disturbance, which causes leaking of CF to the extravesicular region, will be accompanied by increases

in the fluorescence intensity of CF monomers. Experimentally, we only observed negligible changes of ≤ 2% in the presence of **MR5-C5** (Figure 3c) and the other seven **MR**s at 1 μM (Figure S14). But we did obtain fluorescence increases of 35% and 96% at 0.2 and 0.5 μM, respectively, by melittin, a peptide that is capable of forming pores of >1 nm and efficiently lysing the lipid membrane at low concentrations. Based on these findings and those from the SPQ experiments (Figure 3a), it is clear that the observed ion transport activities by **MR**s do arise from their intrinsically high ability to transport potassium ions rather than from **MR**-induced membrane disturbances, including pore formation.

3.5 Ion transport *via* a rotating mechanism

To confirm that these molecular rotors indeed function by using a rotating mechanism for transporting ions, we conducted three sets of control experiments, using (1) **Cr1** that has no crown ether unit (Figure 1), (2) **Cr3** that is structurally similar to **MR5-C5** but with restricted rotation (Figure 4a, b), and (3) the most active **MR5-C5** in DPPC (dipalmitoylphosphatidylcholine that has a high melting point of 41.3 °C) to compare with EYPC (used in our current study) that has a melting point of −2 °C (Figure 4c).

First, as evidenced from the transport curve presented in Figure 2b, **Cr1** is completely inactive in ion transport activity. This indicates that the bis-cholesterol linker itself is unable to self-aggregate to form a membrane-spanning ion channel. In other words, the observed ion transport by molecular rotors is a result of the ion-transporting ability of the crown ether unit.

Second, rather than a rotating mechanism, ion transport may be mostly facilitated by a flip-flop mechanism where the two components (the stator and the crown ether-containing rotator) flip-flop simultaneously. On the one hand, such simultaneous flip-flopping is statistically insignificant, particularly when compared with the scenario where stator and rotator flip-flop at different time points to generate relative angles between them and thus to transport *via* a rotating mechanism. On the other hand, even if this insignificant simultaneous flip-flopping mechanism turns out to be dominant, the crown ether-containing rotator component itself (i.e., the control compound **Cr2**, Figure 1) also must be able to undergo rapid flip-flopping actions to reach a high ion transport efficiency comparable with those observed for **MR**s (0.49–1.37 mol% relative to lipid). Experimentally, however, **Cr2** mediates a negligible ion transport activity of 4% (Figure 2b), while **MR5-C5** exhibits activity as high as 99% at the same concentration of 1 μM. These comparative data rule out the flip-flop action as the main transport mechanism.

Third, given that the rotational barrier of biphenyl group is 2.17 kcal/mol at 0° and 1.79 kcal/mol at 90° [50], which are

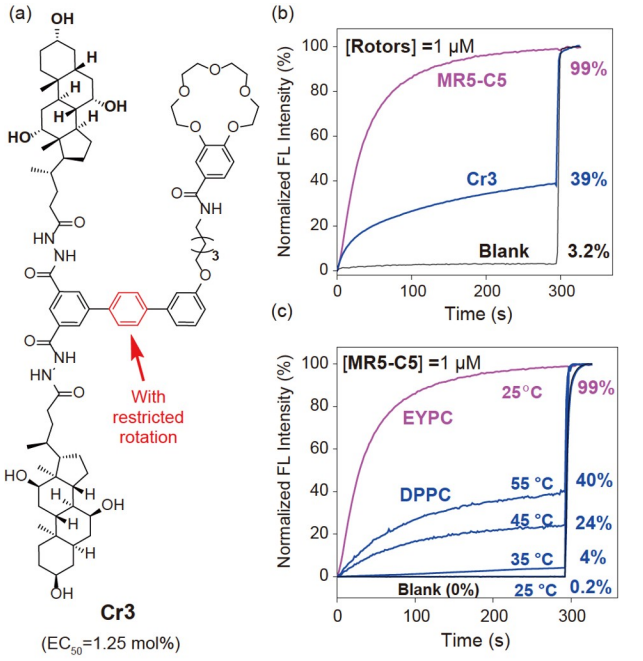

Figure 4 (a) Chemical structure of control compound **Cr3**, having a restricted rotation around the axle; (b) comparative ion transport activities for potassium ion between **MR5-C5** that has an almost freely rotatable triple bond in its axle. (c) Fractional ion transport activities for potassium ion exhibited by **MR5-C5** at 1 μM in EYPC that has a melting point of −2 °C and in DPPC that has a high melting point of 41.3 °C at various temperatures (color online).

higher than the low rotational energy barrier of 0.4–1.1 kcal/mol for the triple bond [49], we designed biphenyl-containing **Cr3** (Figure 4a) that is supposed to have a lower ability in ion transport than **MR**s having the triple bond as the axle. Indeed, **Cr3**, having a more restricted C–C rotation in its axle, displays activity for potassium transport that is about 40% that of structurally similar triple bond-containing **MR5-C5** at 1 μM (Figure 4b). Similarly, the EC_{50} value for potassium ion determined for **Cr3** (1.25 mol%, Figure S15) is about 2.5 times that of **MR5-C5** (0.49 mol%, Table 1). This suggests the flip-flop involving both the stator and the rotator not to be the main mechanism that accounts for the observed ion transport by molecular rotors. Otherwise, molecules **Cr3** and **MR5-C5** should have comparable transport efficiencies. This also suggests that the rotatability of the axle critically influences the ion transport performance of the molecular rotors.

Forth, a negligible transport activity of 0.2% at 25 °C by **MR5-C5** in **DPPC** (melting point = 41.3 °C), when compared with the high ion transport activity of 99% at 25 °C by **MR5-C5** in EYPC (melting point = −2 °C), suggests that the observed ion transport occur through a carrier-like mechanism and cannot be accounted for mainly by a transient transmembrane pathway, self-assembled by stacking multiple crown ethers from multiple identical molecular rotor molecules, through a relay mechanism. This is because the

molecular rotation function is expected to be more sensitive to the relative membrane rigidity or say lipid phase (DPPC *vs*. EYPC) than the intermolecular association involving crown ethers could be.

Lastly, we have carried out the single channel current measurement using the planar lipid bilayer workstation. The fact that our weeklong efforts failed to record any single channel current for **MR5-C5** indicates that molecular rotors function likely in a way more like carriers, which is consistent with the findings from the EYPC/DPPC experiments.

4 Conclusions

In summary, we have proposed and verified the use of molecular rotors as a unique class of unconventional ion transporters. Differing from the carrier or channel mechanisms, they mediate ion transport across the membrane *via* a rotating action. Interestingly, all eight molecular rotors are K^+-selective. More interestingly, regardless of the type of crown ether unit and the length of the rotator, all molecular rotors display high activity in potassium transport, with EC_{50} values of 0.49–1.37 mol% relative to lipid. This certainly suggests the use of a rotating action as a generally effective means for achieving highly efficient transmembrane ion flux. Their highly modular structure allows for engineering the next-generation molecular rotors with ion-specific binding motifs to deliver unconventional ion transporters with high transport selectivity and activity for interesting applications.

Acknowledgements This work was supported by Northwestern Polytechnical University.

Conflict of interest The authors declare no conflict of interest.

Supporting information The supporting information is available online at http://chem.scichina.com and http://link.springer.com/journal/11426. The supporting materials are published as submitted, without typesetting or editing. The responsibility for scientific accuracy and content remains entirely with the authors.

1 Tyska MJ, Warshaw DM. *Cell Motil Cytoskeleton*, 2002, 51: 1–15
2 Asbury CL. *Curr Opin Cell Biol*, 2005, 17: 89–97
3 Wu Y. *J Nucl Acids*, 2012, 2012: 1–14
4 Stoddart JF. *Angew Chem Int Ed*, 2017, 56: 11094–11125
5 Feringa BL. *Angew Chem Int Ed*, 2017, 56: 11060–11078
6 Sauvage JP. *Angew Chem Int Ed*, 2017, 56: 11080–11093
7 Bruns CJ, Stoddart JF. *Acc Chem Res*, 2014, 47: 2186–2199
8 Simpson CD, Mattersteig G, Martin K, Gherghel L, Bauer RE, Räder HJ, Müllen K. *J Am Chem Soc*, 2004, 126: 3139–3147
9 Serreli V, Lee CF, Kay ER, Leigh DA. *Nature*, 2007, 445: 523–527
10 von Delius M, Geertsema EM, Leigh DA. *Nat Chem*, 2009, 2: 96–101
11 Kassem S, Lee ATL, Leigh DA, Markevicius A, Solà J. *Nat Chem*, 2015, 8: 138–143
12 Kudernac T, Ruangsupapichat N, Parschau M, Maciá B, Katsonis N, Harutyunyan SR, Ernst KH, Feringa BL. *Nature*, 2011, 479: 208–211
13 Lewandowski B, De Bo G, Ward JW, Papmeyer M, Kuschel S, Aldegunde MJ, Gramlich PME, Heckmann D, Goldup SM, D'Souza DM, Fernandes AE, Leigh DA. *Science*, 2013, 339: 189–193
14 Paliwal S, Geib S, Wilcox CS. *J Am Chem Soc*, 1994, 116: 4497–4498
15 Chen S, Wang Y, Nie T, Bao C, Wang C, Xu T, Lin Q, Qu DH, Gong X, Yang Y, Zhu L, Tian H. *J Am Chem Soc*, 2018, 140: 17992–17998
16 Ren C, Chen F, Ye R, Ong YS, Lu H, Lee SS, Ying JY, Zeng H. *Angew Chem Int Ed*, 2019, 58: 8034–8038
17 Ye R, Ren C, Shen J, Li N, Chen F, Roy A, Zeng H. *J Am Chem Soc*, 2019, 141: 9788–9792
18 Li N, Shen J, Ang GK, Ye R, Zeng H. *CCS Chem*, 2020, 2: 2269–2279
19 Li N, Chen F, Shen J, Zhang H, Wang T, Ye R, Li T, Loh TP, Yang YY, Zeng H. *J Am Chem Soc*, 2020, 142: 21082–21090
20 Davis JT, Okunola O, Quesada R. *Chem Soc Rev*, 2010, 39: 3843–3862
21 Brotherhood PR, Davis AP. *Chem Soc Rev*, 2010, 39: 3633–3647
22 Benz S, Macchione M, Verolet Q, Mareda J, Sakai N, Matile S. *J Am Chem Soc*, 2016, 138: 9093–9096
23 Gale PA, Davis JT, Quesada R. *Chem Soc Rev*, 2017, 46: 2497–2519
24 Vargas Jentzsch A, Hennig A, Mareda J, Matile S. *Acc Chem Res*, 2013, 46: 2791–2800
25 Montenegro J, Ghadiri MR, Granja JR. *Acc Chem Res*, 2013, 46: 2955–2965
26 Fyles TM. *Acc Chem Res*, 2013, 46: 2847–2855
27 Otis F, Auger M, Voyer N. *Acc Chem Res*, 2013, 46: 2934–2943
28 Gokel GW, Negin S. *Acc Chem Res*, 2013, 46: 2824–2833
29 Gong B, Shao Z. *Acc Chem Res*, 2013, 46: 2856–2866
30 Si W, Xin P, Li ZT, Hou JL. *Acc Chem Res*, 2015, 48: 1612–1619
31 Huo Y, Zeng H. *Acc Chem Res*, 2016, 49: 922–930
32 Su G, Zhang M, Si W, Li ZT, Hou JL. *Angew Chem Int Ed*, 2016, 55: 14678–14682
33 Wei X, Zhang G, Shen Y, Zhong Y, Liu R, Yang N, Al-Mkhaizim FY, Kline MA, He L, Li M, Lu ZL, Shao Z, Gong B. *J Am Chem Soc*, 2016, 138: 2749–2754
34 Lang C, Deng X, Yang F, Yang B, Wang W, Qi S, Zhang X, Zhang C, Dong Z, Liu J. *Angew Chem*, 2017, 129: 12842–12845
35 Ren C, Shen J, Zeng H. *J Am Chem Soc*, 2017, 139: 12338–12341
36 Gong B. *Faraday Discuss*, 2018, 209: 415–427
37 Ren C, Ding X, Roy A, Shen J, Zhou S, Chen F, Yau Li SF, Ren H, Yang YY, Zeng H. *Chem Sci*, 2018, 9: 4044–4051
38 Chen JY, Hou JL. *Org Chem Front*, 2018, 5: 1728–1736
39 Ren C, Zeng F, Shen J, Chen F, Roy A, Zhou S, Ren H, Zeng H. *J Am Chem Soc*, 2018, 140: 8817–8826
40 Li YH, Zheng S, Legrand YM, Gilles A, Van der Lee A, Barboiu M. *Angew Chem Int Ed*, 2018, 57: 10520–10524
41 Zeng F, Liu F, Yuan L, Zhou S, Shen J, Li N, Ren H, Zeng H. *Org Lett*, 2019, 21: 4826–4830
42 Shen J, Fan J, Ye R, Li N, Mu Y, Zeng H. *Angew Chem Int Ed*, 2020, 59: 13328–13334
43 Zeng LZ, Zhang H, Wang T, Li T. *Chem Commun*, 2020, 56: 1211–1214
44 Bai D, Yan T, Wang S, Wang Y, Fu J, Fang X, Zhu J, Liu J. *Angew Chem Int Ed*, 2020, 59: 13602–13607
45 Shen J, Ye R, Romanies A, Roy A, Chen F, Ren C, Liu Z, Zeng H. *J Am Chem Soc*, 2020, 142: 10050–10058
46 Huang WL, Wang XD, Ao YF, Wang QQ, Wang DX. *J Am Chem Soc*, 2020, 142: 13273–13277
47 Malla JA, Umesh RM, Yousf S, Mane S, Sharma S, Lahiri M, Talukdar P. *Angew Chem Int Ed*, 2020, 59: 7944–7952
48 Zheng SP, Huang LB, Sun Z, Barboiu M. *Angew Chem Int Ed*, 2021, 60: 566–597
49 Kottas GS, Clarke LI, Horinek D, Michl J. *Chem Rev*, 2005, 105: 1281–1376
50 Grein F. *J Phys Chem A*, 2002, 106: 3823–3827